Morphological scale-space to differentiate microstructures of food products

Cris L. Luengo Hendriks and Lucas J. van Vliet

Pattern Recognition Group, Faculty of Applied Sciences, Delft University of Technology
Lorentzweg 1, 2628 CJ Delft, The Netherlands

{cris,lucas}@ph.tn.tudelft.nl

Keywords: scale-space, sieves, pore-size distribution, classification, microstructure.

Abstract

We will construct a morphological scale-space using closings at logarithmically sampled scales. From this, we derive a measure for the pore-size distribution. We will apply this method to images of food products, acquired using confocal microscopy, to demonstrate how it can be used to differentiate the microstructure of these products. The microstructures are responsible for important macroscopic properties (firmness, foaming characteristics and mouth-feel). Two applications will be discussed: analysis of monoglycerides, and detection of subtle changes in the microstructure of a dairy product due to different treatments.

1. Introduction

Microstructures of food products determine important macroscopic properties such as firmness, foaming characteristics, and mouth-feel.

In this article, we will measure the pore-size distribution of food products in confocal images using a morphological scale-space. The scale-space is build using a difference of closings at logarithmically sampled scales. This causes the pores to be separated into different levels according to their smallest diameter. Section 2 presents the morphological scale-space. Section 3 shows the results of applying it. First, we will apply it to a synthetic image to demonstrate its capabilities. Then we will apply it to a monoglyceride sample to analyze its pores. Finally, we will use this measure to detect minor changes in the microstructure of a dairy product after some treatment.

2. Methods

2.1. Morphological scale-space

Combining linear scale-space [9, 12] and mathematical morphology [10], we obtain a non-linear scale-space with many interesting properties [2, 3, 6]. Many of the properties of linear scale-space are also valid for morphological scale-spaces (like casualty, regularity, affine invariance, etc. [1]). The main advantage over linear scale-space is the fact that the edges of the objects are not blurred.

Widely used morphological scale-spaces are the M-sieve and N-sieve [4]. A sieve is a cascaded set of non-linear, increasing scale filters that operate in series. It results in the signal being separated into a set of increasing scale components (*granule functions* or *granule images*). Sieves are the non-linear counterpart of the band-pass filter banks (like the Laplacian scale-space). The M_r operator is the result of applying the opening operator γ and then the closing operator ϕ at scale r,

$$M_r\left(f(x)\right)=\phi_r\left(\gamma_r\left(f(x)\right)\right) \quad . \tag{1}$$

The N_r operator applies the same operations in the reverse order. What these operators do is remove all extrema of size smaller than the size r of the structuring element. Since we want to examine the pores, we use only the morphological closing, which will remove minima of size smaller than the structuring element. Our scale-space could therefore be named closing-sieve or pore-sieve.

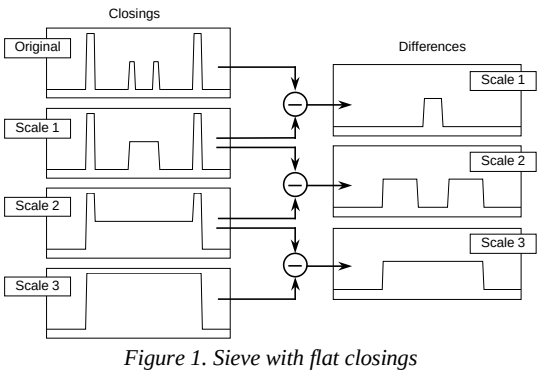

Figure 1. Sieve with flat closings

in: L.J. van Vliet, J.W.J. Heijnsdijk, T. Kielman, P.M.W. Knijnenburg (eds.), Proc. ASCI 2000, 6th Annual Conf. of the Advanced School for Computing and Imaging (Lommel, Belgium, June 14-16), ASCI, Delft, 2000, 289-293.

We construct this scale-space (see figure 1) by first closing the image at all the scales r_i; then we take the difference between subsequent scales. Thus, the granule image at scale r_i is

$$f_{r_i}(x) = \phi_{r_i}\left(f(x)\right) - \phi_{r_{i-1}}\left(f(x)\right) \quad . \qquad (2)$$

Note that, since we use an isotropic structuring element, the morphological closing is determined by the smallest diameter of the pores. Therefore, whenever we mention the size of a pore, what we actually mean is its smallest diameter. This isotropy enables us to apply this method to images of any dimensionality.

Some structures contain different scales. Think about a telephone cable, composed of many bundles, each of which is made out of hundreds of thin wires. The wires are part of two structures at different scales. The morphological scale-space as described earlier is capable of finding both scales. Take as an example the middle pore in figure 1. It is formed by walls of grayvalue *a*, and is inside a region bounded by a higher grayvalue *b*. A closing at some scale will cover the pore with grayvalue *a*. A closing at a larger scale will cover the whole containing region with grayvalue *b*. This results in a single pore being represented at two levels of the scale-space; at the one level with grayvalue *a*, and at the other with grayvalue *b-a*.

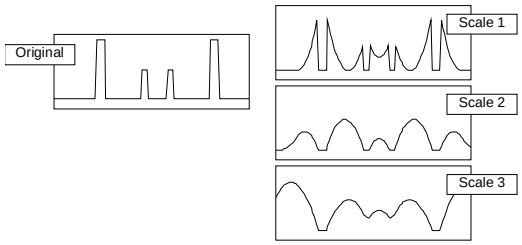

Figure 2. Sieve with parabolic closings.

The figures presented until now suppose a flat structuring element, which is binary, meaning that it is never correctly sampled. This produces problems, especially when a finely sampled scale-space is required (and thus the differences between the required sizes of the structuring elements are small). The obvious solution is to use a parabolic structuring element, which can be sampled more accurately. However, a parabolic closing does not produce the desired result, and a closing-sieve that uses parabolic closings will split a pore into a whole range of levels, which is undesirable here (see figure 2 for an example that clarifies this). The correct solution would be to interpolate the image, so that the flat structuring element can be sampled more densely, reducing the discretization error. Ideally, one would want to downsample the image for the larger structuring elements, so that the discretization error is approximately equal for all levels of the scale-space.

2.2. Pore-size distribution

Once the pores are classified, it is relatively easy to build a size distribution. We propose to use the grayvalue sum at each level as size contribution. To avoid differences in this distribution due to differences in sampling density along the scale axis, it is necessary to divide these quantities by the step size or *granule* (i.e. the difference between the scales at subsequent levels). The pore-size histogram is then given by

$$H(i) = \frac{\sum_x f_{r_i}(x)}{r_i - r_{i-1}} \quad . \qquad (3)$$

Furthermore, by normalizing the distribution we make it invariant to contrast and image size (for this, the scale range has to remain constant)

$$H'(i) = \frac{H(i)}{\frac{1}{N}\sum_k H(k)} \quad . \qquad (4)$$

The question remains on how to sample the scale-space. There is relatively little literature on this topic, and in most articles, one-pixel increments are used as a default solution. It makes sense to use logarithmic sampling, since we might want to distinguish between 3-pixel pores and 4-pixel ones, but not between 100-pixel pores and 101-pixels ones. We will be using two or three samples per octave.

3. Results

3.1. A Synthetic test image

To show that the proposed method works, we apply the closing-sieve to a synthetic image (figure 3-O). It is a superposition of two line patterns, the finer one having squares half the size, and with a grayvalue 50% lower, than the coarser one. The position and orientation of the lines that compose the image have been distorted by white noise (standard deviation of 1 pixel and 1 minute, respectively). We have added a small line pattern to the bottom of the image, with increasing frequency; this is for calibration purposes. Figure 3 shows a four-level closing-sieve resulting from this image. All the holes yield an equal response in two levels, since they all contribute to two different scales. (The sampling of the scales has been chosen to create interesting images.) Figure 4 shows the pore-size distribution for this image, as calculated using the closing-sieve. Note that the jaggedness of the line is due to the size

in: L.J. van Vliet, J.W.J. Heijnsdijk, T. Kielman, P.M.W. Knijnenburg (eds.), Proc. ASCI 2000, 6th Annual Conf. of the Advanced School for Computing and Imaging (Lommel, Belgium, June 14-16), ASCI, Delft, 2000, 289-293.

of the granules. We have applied the sieve on the zoomed image, increasing the scale of the structuring elements proportionally. The thickest line, calculated on the image zoomed by a factor 8, has the smallest discretization error. The differences are mainly in the small-scale part. The difference in the second peak (it becomes larger for 'better' sampled structuring elements) can be attributed to the normalization of the distribution. In figure 4 we have also indicated the granules used for generating the images in figure 3.

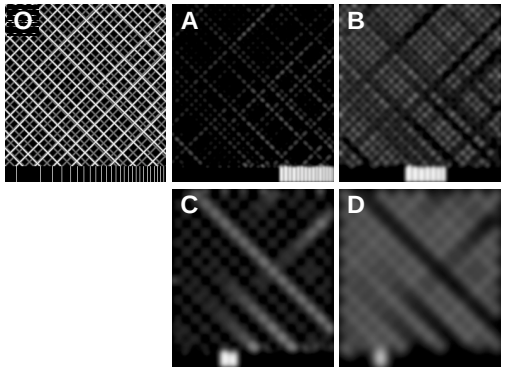

Figure 3. Test image (O) and four levels of the closing-sieve (A-D).

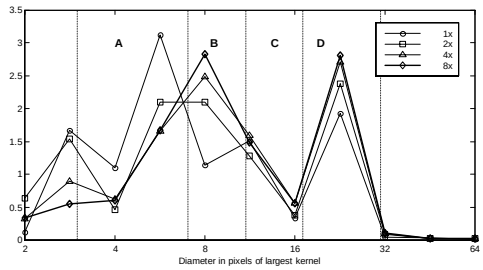

Figure 4. Pore-size distribution using different interpolation factors.

3.2. Monoglyceride

Next, we applied the same method to a slice of a CSLM (Confocal Scanning Laser Microscopy) image. Figure 5 shows a single slice from a monoglyceride sample. Monoglycerides are surfactants used in the production of margarine substitutes [8]. They posses a card-house like structure at microscopic scale, composed of randomly placed planes that enclose water (seen as holes of different sizes). Figure 6 shows the four levels of a closing-sieve, and figure 7 shows the distribution of the pore sizes, along with an indication of the granules shown in figure 6. This graph shows that taking smaller granules does not necessarily improve the sampling of the scale-space, since the error made by the sampling of the structuring element is stressed by the small granules.

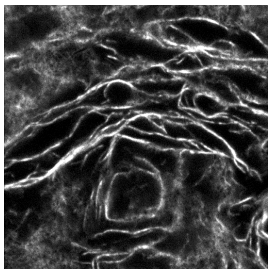

Figure 5. One slice from a CSLM image of a monoglyceride sample.

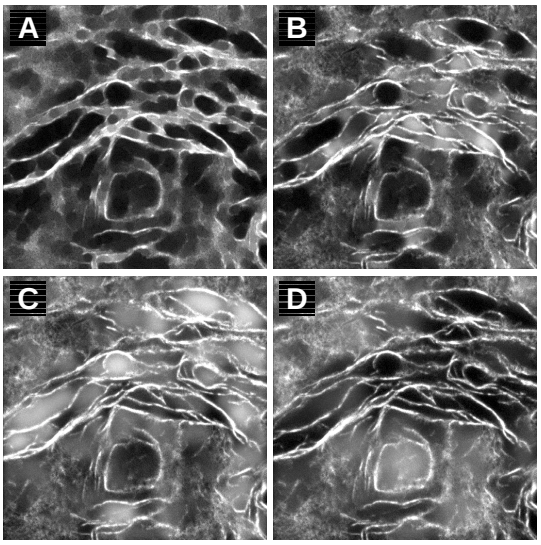

Figure 6. Four levels of a closing-sieve, superimposed over the original image.

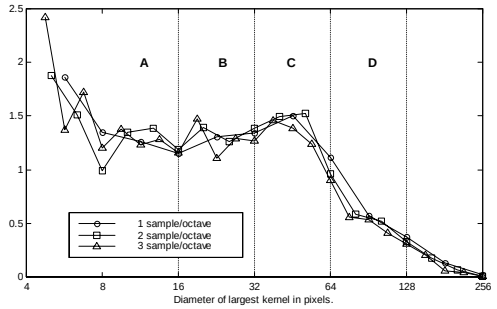

Figure 7. Pore-size distribution using different sampling densities.

3.3. Pore-size distribution in dairy products

The three images in figure 8 are CSLM slices of a dairy product, after different treatments:

- Sample A is the original product.
- Sample B is the same product with a substrate added, which has the side effect of lumping the

in: L.J. van Vliet, J.W.J. Heijnsdijk, T. Kielman, P.M.W. Knijnenburg (eds.), Proc. ASCI 2000, 6th Annual Conf. of the Advanced School for Computing and Imaging (Lommel, Belgium, June 14-16), ASCI, Delft, 2000, 289-293.

proteins together, widening the gaps in between. This yields unfavorable reological properties.

- Sample C is treated with an enzyme that counteracts this effect.

The pores in the image of sample B are supposed to be somewhat larger than in the other two, resulting in different macroscopic properties. The differences between the samples are minimal, and not visible by eye. We apply the closing-sieve to see if it can detect a difference in microstructure.

We have 32 uncorrelated, 256^2 pixel images of each sample. The images are contrast-stretched, making 5% of the pixels black, and 5% white. This is to counteract the clipping that occurred during data acquisition due to a too high dynamic range. The pore-size distribution is calculated for each image. Figure 9 shows the averaged pore-size distributions for the three classes, together with the 95% certainty interval. In this figure, we notice a very small, but statistically relevant difference between class B and the other two classes (which cannot be distinguished from each other).

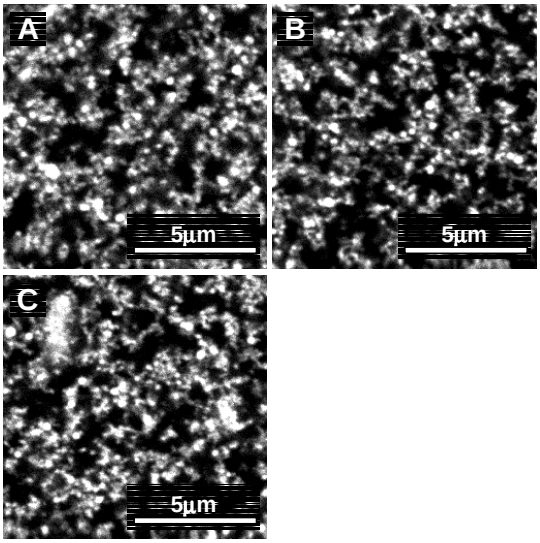

Figure 8. CSLM slices of a milk product after different treatments.

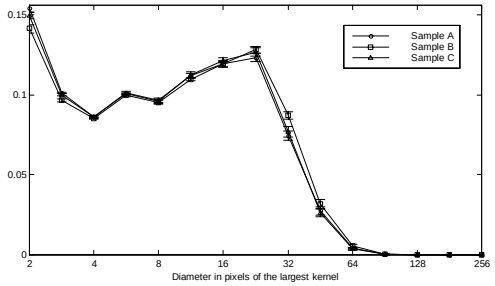

Figure 9. Averaged pore-size distributions for the three samples.

We use the pore-size distribution curve as a 11-dimensional feature vector (we removed the last four points of the distribution), and use a Fisher linear discriminant [5] to map that to a two-dimensional feature-space. In this 2D space, we determine a linear classifier that optimally separates the three classes. However, we have too few objects in this high-dimensional feature-space to divide them into a training set and a test set. Therefore, we use the leave-one-out method to test the accuracy of the classifier. This means that we apply the Fisher linear discriminant and the linear classifier to all the samples except one, which we use to test the classifier. This is repeated until each sample has been used once to test the classification. Table 1 shows the results of this classification in a confusion matrix. The classification results are obvious when one looks at the 2D Fisher mapping in figure 10 (which also shows the weights used by this mapping). Classes A and C overlap for a very large part, whereas class B is somewhat shifted. Class A and C are mistaken for each other about half the time, but it is less frequent that either A or C is mistaken for B and vise-versa.

Table 1. Confusion matrix for the classification of the dairy product.

		objects of class		
		A	**B**	**C**
classified as	**A**	15	3	12
	B	1	22	5
	C	16	7	15

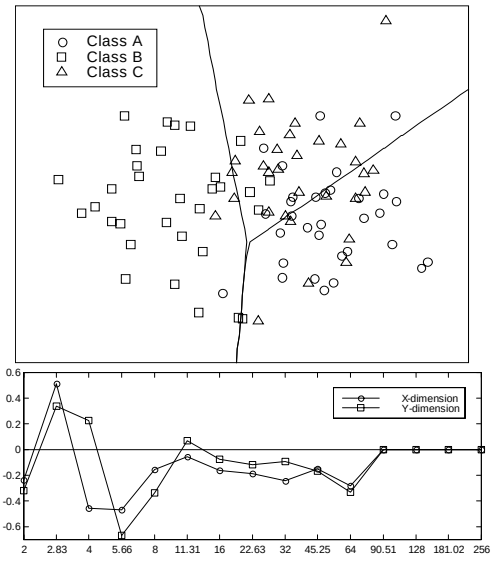

Figure 10. 2D pore-size distribution as mapped by Fisher, and the Fisher weights.

in: L.J. van Vliet, J.W.J. Heijnsdijk, T. Kielman, P.M.W. Knijnenburg (eds.), Proc. ASCI 2000, 6th Annual Conf. of the Advanced School for Computing and Imaging (Lommel, Belgium, June 14-16), ASCI, Delft, 2000, 289-293.

The classification result for the images of each class is a binomial distribution. Figure 11 shows that sample B differs significantly from A and C. The error bars indicate the 95% confidence for the estimated probability. The dotted line is the score that would be obtained by random assignment, which would occur if all samples were identical (indistinguishable by pore-size distribution).

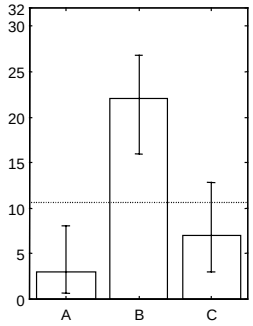

Figure 11. Classification results for images of class B, with estimated 95% confidence.

4. Conclusions

Closing-sieves are best implemented by flat, isotropic structuring elements. Sampling of small isotropic structuring elements causes a large discretization error. Interpolation of the acquired images allows an increase of the structuring element by the same factor, which effectively reduces the discretization effects of the flat structuring elements.

Applying the closing-sieve to CSLM images of food products shows that it allows segmentation of holes and classification of hole size in a card-house like structure such as monoglyceride samples. Subtle differences in the microstructure of "treated" dairy products have been detected by classifying the measured pore-size distributions using a Fisher mapping.

Acknowledgements

We would like to thank Geert van Kempen, Han Blonk and Liesbeth Bouwens at Unilever Research Vlaardingen for the discussions and the data sets. This research is partially supported by the Innovative Research Program (IOP), under project number IBV98006.

For the purposes of the research presented here, we have made use of the software packages DIPlib [11] and PRTOOLS [7].

References

[1] L. Alvarez and J.-M. Morel, "Morphological Approach to Multiscale Analysis: From Principles to Equations," in *Geometry-Driven Diffusion in computer Vision*, M. A. Viergever, Ed. Dordrecht: Kluwer Academic Publishers, 1994.

[2] J. A. Bangham, T. G. Campbell, and R. V. Aldridge, "Multiscale Median and Morphological Filers for 2D Pattern Recognition," *Signal Processing*, vol. 38, pp. 387-415, 1994.

[3] J. A. Bangham, P. Chardaire, C. J. Pye, and P. D. Ling, "Multiscale Nonlinear Decomposition: The Sieve Decomposition Theorem," *IEEE Transactions on Pattern Analysis and Machine Intelligence*, vol. 18, pp. 529-539, 1996.

[4] J. A. Bangham, P. D. Ling, and R. Harvey, "Scale-Space From Nonlinear Filters," *IEEE Transactions on Pattern Analysis and Machine Intelligence*, vol. 18, pp. 520-528, 1996.

[5] C. M. Bishop, *Neural Networks for Pattern Recognition*. Oxford: Oxford University Press, 1995.

[6] M.-H. Chen and P.-F. Yan, "A Multiscaling Approach Based on Morphological Filtering," *IEEE Transactions on Pattern Analysis and Machine Intelligence*, vol. 11, pp. 694-700, 1989.

[7] PRTOOLS 2.2, Pattern Recognition Group, Delft, 1998. http://www.ph.tn.tudelft.nl/~duin/... PRTOOLS.html.

[8] I. Heertje, E. C. Roijers, and H. A. C. M. Hendrikx, "Liquid Crystalline Phases in the Structuring of Food Products," *Lebensmittel-Wissenschaft und Technologie*, pp. 387-396, 1998.

[9] J. J. Koenderink, "The Structure of Images," *Biological Cybernetics*, pp. 363-370, 1984.

[10] J. Serra, *Image Analysis and Mathematical Morphology*. London: Academic Press, 1982.

[11] DIPlib 1.2, Pattern Recognition Group, Delft, 1999. http://www.ph.tn.tudelft.nl/DIPlib/.

[12] A. P. Witkin, "Scale-space Filtering," presented at the Eighth International Joint Conference on Artificial Intelligence, Karlsruhe, Germany, 1983.